

# Spin Weyl Topological Insulators

Rafael González-Hernández<sup>1,\*</sup> and Bernardo Uribe<sup>2,†</sup>

<sup>1</sup>*Departamento de Física y Geociencias, Universidad del Norte,  
Km. 5 Vía Antigua Puerto Colombia, Barranquilla 080020, Colombia*

<sup>2</sup>*Departamento de Matemáticas y Estadística, Universidad del Norte,  
Km. 5 Vía Antigua Puerto Colombia, Barranquilla 080020, Colombia*

(Dated: January 18, 2024)

The quantum nature of electron spin is crucial for establishing topological invariants in real materials. Since the spin does not in general commute with the Hamiltonian, some of the topological features of the material can be extracted from its study. In insulating materials, the spin operator induces a projected operator on valence states called the spin valence operator. Its spectrum contains information with regard to the different phases of the spin Chern class. If the spin valence spectrum is gapped, the spin Chern numbers are constant along parallel planes thus defining spin Chern insulating materials. If the spin valence spectrum is not gapped, the changes in the spin Chern numbers occur whenever this spectrum is zero. Materials whose spin valence spectrum are gapless will be denoted spin Weyl topological insulators and its definition together with some of their properties will be presented in this work. The classification of materials from the properties of the spin valence operator provides a new characterization which complements the existing list of topological invariants.

## I. INTRODUCTION

Topological insulators exhibit a unique electronic structure where the bulk of the material remains insulating due to the presence of a large energy band gap, while the surface or edge states emerge when the material interfaces with a trivial insulator.<sup>1,2</sup> This feature of a material can be related to classical topological invariants associated to the vector bundle of occupied states (valence eigenstates) such as the first Chern number in the 2D case and the Chern-Simons invariant ( $\theta$ -term) in the 3D case.<sup>3-5</sup>

The characterization of the topological nature of a material from first-principles calculations has been extensively studied, and several procedures have been established to extract its features, such as Wilson loop calculations,<sup>6,7</sup> eigenvalues of crystal symmetry operators<sup>8,9</sup> and elementary band representation of valence bands,<sup>10,11</sup> among others. In this work we propose an alternative strategy to detect the topological nature of a material which is based on the topological properties of the spin operator. The noncommutativity of the spin operator with the Hamiltonian permits to infer relevant information of the material from the spectrum of the spin operator once it is restricted to the valence bands.<sup>12</sup> The geometrical and topological properties of this spectrum follow the same structural behavior as the ones from the energy spectrum.<sup>13,14</sup> Gapless systems will then have Weyl points (spin Weyl points), and the understanding of the location and the chirality of these points is the key ingredient underlying our proposal for a new indicator.

Our proposal for an indicator enhancing the known classification of topological materials is called the spin

invariants vector. This vector has seven integer numbers where the first number counts the number of spin Weyl points with positive chirality and the next six are the Chern numbers of the negative spin valence eigenvalues across the planes  $k_l=0, \pi$  for  $l=x, y, z$ . The first number is denoted spin Weyl indicator and it is zero only when the spin valence spectrum is gapped. In this case the spin Chern numbers are constant across parallel planes and the next six coordinates simply encode these constant Chern numbers; in this case the material is a spin Chern insulator when some Chern number is non zero, or a spin insulator if all Chern numbers are trivial. If the spin Weyl indicator is not zero, then the spin valence spectrum is gapless and the Chern number across parallel planes may differ, we call these materials spin Weyl topological insulators. The next six coordinates provide the information of the Chern numbers across the six planes  $k_l=0, \pi$ , and the spin Weyl indicator measures the total positive change of Chern number across parallel planes.

The parity of the spin Weyl indicator is precisely the Fu-Kane-Mele invariant, and in the case of the spin Weyl indicator being even, it provides an enhancement for the detection of weak and fragile topological phases.<sup>15</sup>

In order to understand the features of the spin invariant vector, we analyze the behavior of the spin valence operator in the 3D Bernevig-Hughes-Zhang (BHZ) model,<sup>16</sup> as well as in particular tight-binding Hamiltonian.<sup>17</sup> In the 3D BHZ model we obtain five different topological phases depending on one parameter. Two trivial insulator phases, two strong topological insulator phases and one spin Weyl topological insulator phase. This last phase exhibits a gapless spin valence spectrum with a total of four spin Weyl points. Its topological nature is also inferred from the change of spin Chern number from -1 in  $k_z = 0$  to 1 in  $k_z = \pi$  (see Fig 2). The tight-binding Hamiltonian exhibits a strong topological insulator phase with two Weyl points and with spin invariant

\* rhernandezj@uninorte.edu.co

† bjongbloed@uninorte.edu.co

vector (1|10-1000). Finally, we calculate the properties of the spin valence spectrum in materials  $\text{Bi}_2\text{Te}_3$ , Bi and  $\text{SnTe}$ , thus characterizing  $\text{Bi}_2\text{Te}_3$  as a strong topological insulator, Bi as a spin Chern insulator and  $\text{SnTe}$  as a spin Weyl topological insulator. All three materials exhibit a non-zero spin Hall Effect, suggesting that the appearance of the phenomenon is predicted by the non-triviality of the spin Chern numbers.

The spin Chern numbers thus become a customized tool for the distinction and classification of topological insulators. This ansatz was originally put forward by Prodan<sup>12</sup> who showed the robustness of the spin Chern numbers and carried out an extensive analysis of the properties of the spin valence spectrum. The implications of the robustness of the spin Chern numbers have been explored by other authors,<sup>18</sup> and in the case of 3D insulating materials, a comprehensive analysis of both theoretical and computational aspects has been studied by several authors.<sup>19,20</sup> By introducing nested spin-resolved Wilson loops and layer constructions, Lin et al.<sup>20</sup> studied the behavior of the spin Chern numbers across parallel planes in the BZ, thus describing topological properties of these numbers while detecting the presence of spin Weyl points. This analysis allowed Lin et al.<sup>20</sup> to propose a novel method for further classifying topological insulating phases.

In the present paper we further explore the properties of the spin valence spectrum in 3D insulating materials and we propose a new indicator that can effectively identify 3D topological insulating phases. This newly established indicator, based on the spin properties, offers valuable insights into the fundamental understanding and potential applications of topological materials.

## II. INVARIANTS OF TOPOLOGICAL INSULATORS

The mathematics behind the theory of topological invariants in insulating materials has been extensively studied.<sup>21,22</sup> Several methods for detecting topological invariants of a prescribed Hamiltonian have been established and the construction of a comprehensive list of all possible indicators for such invariants is currently an active area of research.<sup>23,24</sup>

The importance of these topological invariants lies in the amazing relation that some of them have with certain electromagnetic properties of materials. For instance, in 2D insulators, the Chern number of the occupied states provides the quantization of the Anomalous Hall Effect,<sup>25</sup> and in 3D insulators with Time Reversal Symmetry (TRS), the non-triviality of the Fu-Kane-Mele invariant (FKM) provides an indicator of a strong topological insulating type;<sup>26</sup> just to mention a few.

The main line of thought underlying the existence of the topological invariants in insulators goes as follows. The Hamiltonian of the periodic system provides a Hermitian operator acting on parametrized vectors over the

Brillouin Zone (BZ):

$$\hat{H} : \Gamma(\mathbb{C}^N \times B) \rightarrow \Gamma(\mathbb{C}^N \times B), \quad (1)$$

here  $N$  is the number of bands,  $B$  denotes the BZ and  $\Gamma$  denotes the space of sections of the trivial complex vector bundle  $\mathbb{C}^N \times B$ .

Whenever there is an energy gap at the Fermi level on the eigenvalues of the Hamiltonian, we say that the material is insulating. The insulating condition permits to separate the valence states from the conducting ones. This separation at the level of vector bundles defines the partition

$$\mathbb{C}^N \times B \cong E^{val} \oplus E^{cond} \quad (2)$$

where the sections of the bundle  $E^{val}$  are generated by the valence eigenvectors of the Hamiltonian  $\{|\psi_i\rangle\}_{i=1}^{n_{occ}}$ , where  $n_{occ}$  indicates the number of occupied bands which is the rank of  $E^{val}$ .

Since  $E^{val}$  is a complex vector bundle over the BZ, we may assign to it the topological invariants that it defines in the complex K-theory groups. The only interesting invariant that appears here, besides the rank of the vector bundle, is the first Chern class. This first Chern class  $c_1 := c_1(E^{val})$  can be evaluated on planes inside the BZ and the associated numbers can be determined.

If the first Chern class  $c_1$  is not zero, the material is called a Chern insulator. In the 2D case it provides the quantization of the Anomalous Hall Effect and several materials exhibit this property.<sup>27</sup> On the other hand, 3D materials with a Chern Insulating property have been elusive to detect and until now none single 3D material exhibits this property.

By incorporating geometrical and physical symmetries of the Hamiltonian into the analysis, more specific information regarding the topological invariants can be deduced. If the system preserves TRS ( $\mathbb{T}$ ), and we are in the spin orbit coupling (SOC) environment with  $\mathbb{T}^2 = -1$ , then the FKM invariant provides an indicator of the strong topological insulating property.<sup>26,28</sup> If the symmetry preserved is  $C_2\mathbb{T}$ , a combination of a  $180^\circ$  rotation and TRS, then an indicator of being an axion insulator is the Stiefel-Whitney class of the  $C_2\mathbb{T}$  invariant real vector bundle of  $E^{val}$  restricted to the planes fixed by  $C_2\mathbb{T}$ .<sup>29</sup>

It is important to notice that every extra crystal symmetry will induce topological invariants. Sometimes the invariants already appeared due to another symmetry, but some other times the invariant is new and may or may not imply the existence of invariants of other symmetries. The task of finding a complete set of indicators for all geometrical symmetries is an ongoing subject of research.

Besides the geometrical symmetries, there are also the physical symmetries. These are the ones that come from the fact that we are dealing with a quantum mechanical system. One such symmetry is the spin, and incorporating it into the analysis of topological invariants has been very fruitful.<sup>12</sup> In what follows we will study some of the

topological invariants which can be extracted when the spin operator acts in the occupied wave function space.

### III. SPIN WEYL INDICATOR

If the spin operator  $\hat{S}_z$  does not commute with the Hamiltonian, we cannot expect to simultaneously diagonalize it with the Hamiltonian. In order to obtain a symmetry of the vector bundle  $E^{val}$ , we compose the action of the spin operator with the projection onto the occupied states:

$$\hat{S}_z^{val} : \Gamma(E^{val}) \rightarrow \Gamma(E^{val}) \quad (3)$$

$$\varphi \mapsto \pi^{val} \circ \hat{S}_z(\varphi); \quad (4)$$

here  $\pi^{val} : \Gamma(\mathbb{C}^N \times B) \rightarrow \Gamma(E^{val})$  is the projection operator  $\sum_{i=1}^{n_{occ}} |\psi_i\rangle\langle\psi_i|$ .

We call the operator  $\hat{S}_z^{val}$  the spin valence (SV) operator and one could see it as a physical symmetry of the bundle  $E^{val}$  of occupied states. This SV operator can be diagonalized, and its spectrum can be studied with exactly the same tools as the ones used to understand the spectrum of the Hamiltonian. We have used the  $\hat{S}_z^{val}$  component for the spin operator, but it can be generalized to include other components.

Note that the SV spectrum takes values in the interval  $[-1, 1]$  (in  $\hbar/2$  units), and moreover, that an eigenvalue of zero means that there is a combination of occupied states whose spin lies completely on the unoccupied states. Hence it is important to measure whether the SV spectrum crosses the zero value or not, and two different scenarios appear (See Figure 1).

#### A. Gapped Spin valence spectrum

If the SV spectrum is gapped at zero, then we can partition the vector bundle  $E^{val}$  into two different vector bundles:

$$E^{val} \cong E_{s_z^+}^{val} \oplus E_{s_z^-}^{val} \quad (5)$$

where  $E_{s_z^+}^{val}$  and  $E_{s_z^-}^{val}$  denote respectively the positive and negative SV eigenstates.

The topological invariants associated to these two complex vector bundles is the first Chern classes

$$c_1^{s_z^\pm} := c_1(E_{s_z^\pm}^{val}) \quad (6)$$

and since

$$c_1 = c_1^{s_z^+} + c_1^{s_z^-}, \quad (7)$$

the new invariant is usually defined as half the difference between the two Chern classes:

$$c_1^{s_z} = \frac{1}{2} (c_1^{s_z^+} - c_1^{s_z^-}). \quad (8)$$

This Chern class is called the spin Chern class, and together with the total first Chern class  $c_1$ , determines uniquely the first Chern class of both the positive and the negative SV states.

When TRS is preserved, the vector bundles  $E_{s_z^+}^{val}$  and  $E_{s_z^-}^{val}$  are isomorphic via the antiunitary transformation defined by  $\mathbb{T}$ . In this case  $c_1^{s_z^+} = -c_1^{s_z^-}$  and therefore the spin Chern class  $c_1^{s_z}$  is the invariant preserved. In 2D materials whose spin almost commutes with the Hamiltonian, the spin Chern number is a good indicator for the Quantum spin Hall Effect. These materials are called quantum spin Hall insulators (QSHI) and they include both functionalized and pristine antimonene and bismuthene 2D materials.<sup>30,31</sup>

In 2D systems Chern classes are uniquely determined by the Chern number, namely the integration of the Chern class on the whole BZ. While on 3D systems they are determined by the integrals along all closed surfaces in the BZ. The value of this integral over any closed surface  $surf$  is the Chern number associated with the surface:

$$c_1^{s_z^\pm}(surf) := \int_{surf} c_1(E_{s_z^\pm}^{val}). \quad (9)$$

The spin Chern numbers are usually associated with planes of the form  $k_l=0, \pi$ , and in the case of a gapped SV spectrum, these numbers are constant along parallel planes. The spin Chern number can only vary on parallel planes whenever the SV spectrum is gapless, thereby indicating the presence of spin Weyl (SW) points.

#### B. Gapless Spin valence spectrum

Whenever the SV spectrum is not gapped, we cannot partition the occupied states into positive and negative SV eigenvectors all across the BZ. But outside the points in momentum space where the SV eigenvalue is zero, this partition can be performed.

Call **Spin Weyl (SW) points** the points in momentum space where there is a zero SV eigenvalue. Around each SW point  $\mathbf{k}$ , a 2D sphere  $S_\epsilon(\mathbf{k})$  of small radius  $\epsilon > 0$  could be defined. The vector bundle of occupied states restricted to this sphere splits into positive and negative SV eigenvectors. Therefore we could associate to the SW point the Chern number of the negative SV eigenvectors restricted to the sphere.

Mimicking the definition of the chirality of Weyl points of the Hamiltonian, we define the **spin Chirality** of the SW point  $\mathbf{k}$  as follows:

$$\chi^{s_z}(\mathbf{k}) := c_1^{s_z^-}(S_\epsilon(\mathbf{k})). \quad (10)$$

By the Nielsen-Ninomiya Theorem,<sup>32</sup> the sum of the spin Chiralities of all SW points is zero:

$$\sum_{\mathbf{k} \in SW} \chi^{s_z}(\mathbf{k}) = 0, \quad (11)$$

where  $SW$  denotes the finite set of spin Weyl points in a generic Hamiltonian.

Therefore the maximum Berry curvature flux of the negative SV states is given by the sum of all positive spin chiralities. Simply enclose with a closed surface the spin Weyl points with positive chirality, and by Gauss' law, the total flux is the sum of the chiralities inside the surface.

We claim that this maximum Berry curvature flow of the negative SV states is a topological indicator of the system. We therefore propose to define the **spin Weyl indicator** (SWI) of the system as the sum of the positive chiralities of all SW points:

$$\text{SWI} := \frac{1}{2} \sum_{\mathbf{k} \in SW} |\chi^{s_z}(\mathbf{k})|. \quad (12)$$

The formula above simply computes the sum of the absolute value of all chiralities and divides by two. This way there is no need to distinguish the positive chiralities from the negative ones.

The SWI is a natural number that encodes topological information about the system. For instance, in the presence of TRS or TRS composed with a 2-fold rotation, the parity of the SWI is respectively equivalent to the FKM invariant<sup>26,28</sup> or to the value of the  $\theta$ -term.<sup>29</sup> Whenever the SWI is zero, the projected spin operator is gapped, and the material can be classified as spin Chern insulator if any spin Chern number is not zero. Whenever SWI is even, the material might be endowed with weak or fragile topological phases.

Calculating the SWI by detecting the SW points together with their chiralities might be cumbersome. Alternatively, we propose to calculate the Chern number of the negative SV eigenstates across planes perpendicular to a given axis. By choosing the  $k_l$ -axis for  $l = x, y, z$  we calculate and plot the function

$$\text{SCN} : [-\pi, \pi] \rightarrow \mathbb{Z} \quad (13)$$

$$t \mapsto c_1^{s_z}(k_l = t). \quad (14)$$

This function increases and decreases by integer values whenever SW points are crossed, and the total amount of positive changes is precisely the SWI. We will call this function the signal of the **Spin Chern number (SCN)**; cf.<sup>19</sup>

The SCN signal has been plotted in the 3D Bernevig-Hughes-Zhang (BHZ) model in Fig. 2, in the Tight-Binding (TB) model of pristine pyrochlore in Fig. 4c) and in real materials  $\text{Bi}_2\text{Te}_3$  and  $\text{SnTe}$  in Fig. 5 c) and c') respectively. In all these cases the value of the SWI can be deduced from the signal of the SCN in the BZ.

### C. Spin invariants vector

It is important to notice that the SWI cannot be deduced solely from the spin Chern numbers of the planes

$k_l = 0, \pi$  with  $l = x, y, z$ . The material  $\text{SnTe}$  has spin Chern number equal to 2 along the planes  $k_l = 0, \pi$  for  $l = x, y$  and 0 along the planes  $k_z = 0, \pi$  (see Fig. 5 c')), while its SWI equals 8.

A coherent set of invariants associated with the SV operator should therefore include the spin Chern numbers along the preferred planes plus the value of the SWI. Hence we propose to define the **spin invariants vector** as the array of seven integer numbers

$$(n|n_x^0, n_x^\pi, n_y^0, n_y^\pi, n_z^0, n_z^\pi) \quad (15)$$

where  $n = \text{SWI}$  and  $n_l^w = c_1^{s_z}(k_l = w)$ .

The spin invariants vector will provide the information necessary to determine the spin topological classification presented in Fig. 1. The zero vector represents a spin insulator, a vector with  $n = 0$ , which is moreover non-trivial, represents a spin Chern insulator, and a vector with  $n \neq 0$  represents a spin Weyl topological insulator.

## IV. 3D BHZ MODEL

The 2D Bernevig-Hughes-Zhang (BHZ) two band model (upper left  $2 \times 2$  matrix of (16)) for a spin topological insulator<sup>16</sup> can be used to construct a four band Hamiltonian in 3D where two opposite copies of the 2D BHZ model are superposed (matrix of (16) with  $D = 0$ ). In order to obtain a change of phase for the 2D layers, an off-diagonal term  $D$  depending on  $k_z$  is added thus obtaining one version of the 3D BHZ Hamiltonian

$$H_{\text{BHZ}}(\mathbf{k}) = \begin{pmatrix} M & A & 0 & D \\ A^* & -M & D & 0 \\ 0 & D & M & -A^* \\ D & 0 & -A & -M \end{pmatrix} \quad (16)$$

where

$$M = M_0 - B_0 (\cos(k_x) + \cos(k_y) + \cos(k_z)), \quad (17)$$

$$A = A_0 (\sin(k_x) + i \sin(k_y)), \quad (18)$$

$$D = D_0 \sin(k_z). \quad (19)$$

This Hamiltonian is written in a basis given by the states  $|F \uparrow\rangle, |H \uparrow\rangle, |F \downarrow\rangle, |H \downarrow\rangle$ , in that order, and it models a phase transition of a 2D topological insulator. In what follows we will show that changes in the value of  $\frac{M_0}{B_0}$  induce five different insulating phases for this 3D model, where each phase change is marked by the closure of the energy band gap.

For  $3 < |\frac{M_0}{B_0}|$  it is a trivial insulator, for  $1 < |\frac{M_0}{B_0}| < 3$  we have an STI whose SWI is 1, and for  $-1 < \frac{M_0}{B_0} < 1$  we have SWTI whose SWI is 2. These phases are illustrated in Figure 2.

The degenerate Eigenvalues of the Hamiltonian are  $E = \pm \lambda$  with

$$\lambda = \sqrt{(M^2 + |A|^2 + D^2)}, \quad (20)$$

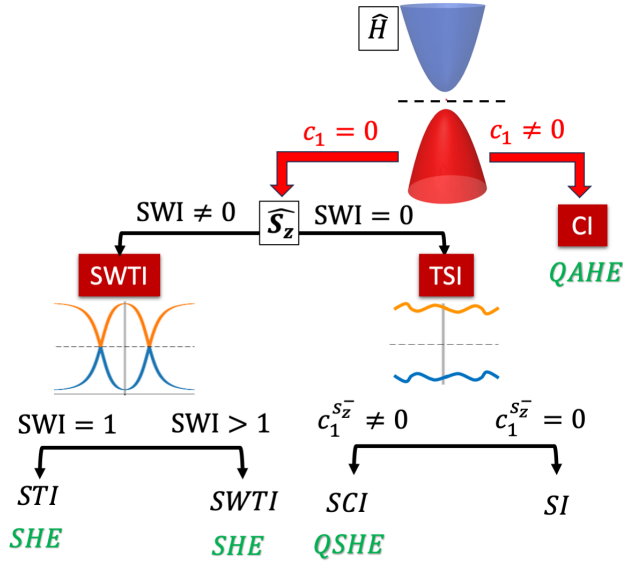


FIG. 1. Topological classification of 3D insulators using Chern classes and the SWI (spin Weyl indicator). If the total Chern class  $c_1$  of the valence states is non-trivial, there is a plane where the Chern number is not zero. In this case the material is a Chern insulator (CI) and the anomalous Hall effect is quantized (QAHE). When the total Chern class of the valence states is trivial, then the SWI number indicates whether the spin Chern numbers vary along parallel planes. Whenever the SWI is trivial, then there are no SW points and therefore the spin Chern numbers do not vary; these materials will be called topological spin insulators (TSI). In this case if the spin Chern class  $c_1^{s_z^-}$  is trivial, the material is a spin insulator (SI), otherwise the material is a spin Chern insulator (SCI) and has a quantized spin Hall effect (QSHE). Whenever the SWI is not zero, the spin Chern numbers vary along parallel planes and therefore the spin Chern numbers along the planes  $k_l = 0, \pi$  do not constitute a complete topological indicator of the material. The case of the SWI being 1 corresponds with most models whose FKM invariant is non-trivial; these are the strong topological insulators (STI)s. Materials whose SWI is non-trivial will be denoted spin Weyl topological insulators (SWTI); these materials show a spin Hall effect (SHE) inside the energy band gap.

and one choice of eigenvectors are:

$$\nu_1 = ((M - \lambda), A^*, 0, D) \quad (21)$$

$$\nu_2 = (A, -(M + \lambda), D, 0) \quad (22)$$

$$\nu_3 = ((M + \lambda), A^*, 0, D) \quad (23)$$

$$\nu_4 = (A, -(M - \lambda), D, 0). \quad (24)$$

The energy spectrum is gapless only when  $M = A = D = 0$  and this only happens whenever  $\frac{M_0}{B_0} = -3, -1, 1, 3$ . For any other choice of  $\frac{M_0}{B_0}$  the energy spectrum is gapped.

Note that the valence states  $\nu_1$  and  $\nu_2$  are not linearly independent as presented above; nevertheless this simple presentation of the eigenvectors permit us to deduce an important result that it will be outlined in what follows.

## A. Spin Weyl points

The spin operator  $\hat{S}_z$  in this case is the diagonal matrix  $\text{diag}(1, 1, -1, -1)$ , and we may restrict the spin operator only to the valence states. If  $\psi_j$  are the eigenvectors of the Hamiltonian forming a unitary base (norm one and perpendicular to one another), then the SV matrix is defined as follows:

$$(M_{s_z})_{ij} = \langle \psi_i | \hat{S}_z | \psi_j \rangle \quad i, j \in \{1, 2\}. \quad (25)$$

The eigenvalues of the SV matrix give us the SV spectrum. Whenever there is an SV eigenvalue gap, we could separate the positive states from the negative states, and we could find the topological invariants for each group of SV eigenstates. Where the SV spectrum is not gapped, a spin Chern number transition occurs in the BZ. Let us show that this indeed is what happens in the 3D BHZ Hamiltonian.

The SV eigenvalues vanish whenever the whole SV matrix vanishes. Note that in this case, we could use the degenerate basis  $\{\nu_1, \nu_2\}$  of Eqns. (21) and (22) in order to solve the equations

$$\langle \nu_i | \hat{S}_z | \nu_j \rangle = 0 \quad i, j \in \{1, 2\}. \quad (26)$$

The equations become

$$\langle \nu_1 | \hat{S}_z | \nu_2 \rangle = 2A\lambda = 0 \quad (27)$$

$$\langle \nu_2 | \hat{S}_z | \nu_1 \rangle = 2A^*\lambda = 0 \quad (28)$$

$$\langle \nu_1 | \hat{S}_z | \nu_1 \rangle = (M - \lambda)^2 + |A|^2 - D^2 = 0 \quad (29)$$

$$\langle \nu_2 | \hat{S}_z | \nu_2 \rangle = (M + \lambda)^2 + |A|^2 - D^2 = 0 \quad (30)$$

and therefore  $A = 0$  and  $M = 0$ . The SW points on each of the three non-trivial phases can be seen in Table I. In this Hamiltonian the SW points come in pairs with opposite chirality due to the TRS.

Now let us find the linear expansion on  $\mathbf{k}$  of the SV eigenvalues around the SW points. For this end we need to find an orthonormal basis of the valence states, and instead of doing it in complete generality, we will only calculate the linear  $k_z$  expansion centered on the point  $(0, 0, \cos^{-1}(\frac{M_0}{B_0}))$  for the phase  $-1 < \frac{M_0}{B_0} < 1$ .

Restricting the system to  $k_x = 0 = k_y$  we find that the valence unitary eigenvectors for the Hamiltonian  $H_{BHZ}(\mathbf{k})$  for  $\mathbf{k} = (0, 0, \cos^{-1}(\frac{M_0}{B_0}))$  are:

$$\psi_1 = \frac{(M - \lambda, -D, -(M - \lambda), D)}{\sqrt{2(M - \lambda)^2 + 2D^2}} \quad (31)$$

$$\psi_2 = \frac{(M - \lambda, D, M - \lambda, D)}{\sqrt{2(M - \lambda)^2 + 2D^2}}. \quad (32)$$

$$(33)$$

The SV matrix becomes

$$M_{s_z} = \frac{(M - \lambda)^2 - D^2}{(M - \lambda)^2 + D^2} \sigma_x = -\frac{M}{\lambda} \sigma_x \quad (34)$$

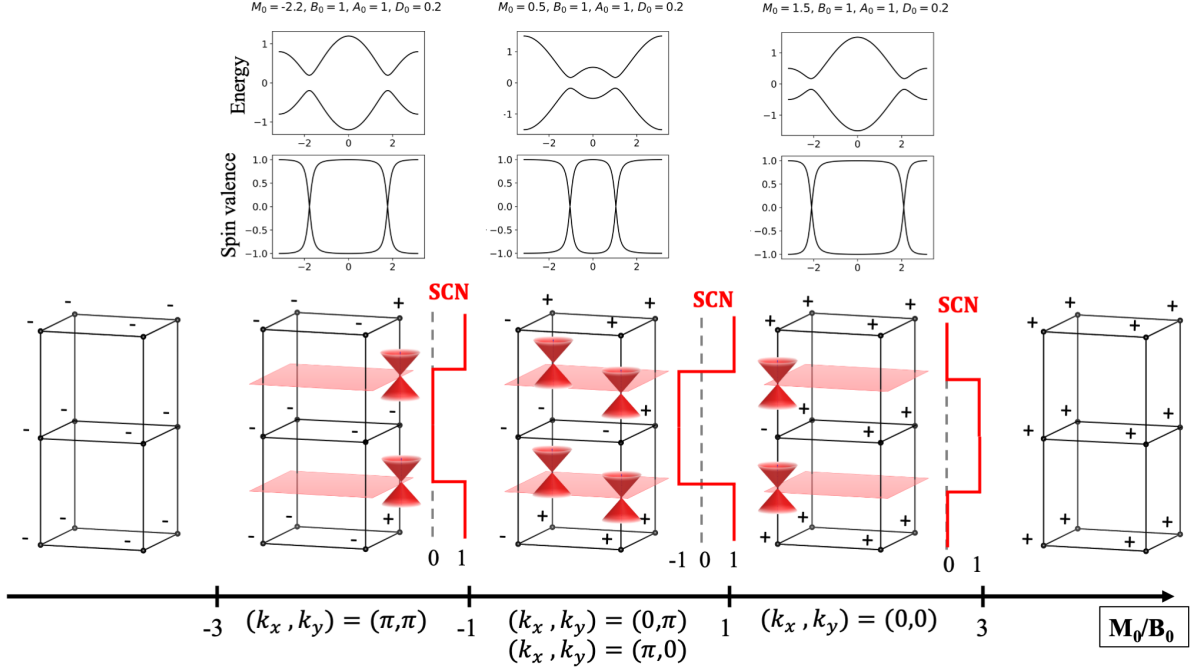


FIG. 2. Five phases of the 3D BHZ Hamiltonian of Eqn. (16). For  $\frac{M_0}{B_0} = -3, -1, 1, 3$  the Hamiltonian is gapless, and for other values of  $\frac{M_0}{B_0}$  the Hamiltonian is gapped. For  $|\frac{M_0}{B_0}| > 3$  the system is a trivial insulator, for  $1 < |\frac{M_0}{B_0}| < 3$  it is a Strong TI with SWI=1 and for  $|\frac{M_0}{B_0}| < 1$  it is a SWTI with SWI=2. The cones are located where the spin valence eigenvalues are zero, and this occurs along axis parallel to the  $k_z$  axis: in the first non-trivial phase they are on  $(k_x, k_y) = (0, 0)$ , on the second non-trivial phase on  $(k_x, k_y) = (0, \pi)$  and  $(k_x, k_y) = (\pi, 0)$ , and on the third non-trivial phase on  $(k_x, k_y) = (\pi, \pi)$ . The signs on the TRIMs denote the eigenvalues of the inversion operator on the negative spin valence eigenstate. The step functions on the right of each BZ is the plot of the Chern number of the negative spin valence eigenstate on the planes  $k_z = t$  when  $t$  varies from  $-\pi$  to  $\pi$ . The Energy and spin valence plots vs. the appropriate axis parallel to the  $k_z$ -axis in the three non-trivial phases are shown for specific choices of structural constants. The spin Weyl points can be seen in all of them.

Phase	Spin Weyl points	Spin Chern number	Spin Weyl indicator	FKM invariant	Spin invariants vector
$-3 < \frac{M_0}{B_0} < -1$	$(\pi, \pi, \pm \cos^{-1}(\frac{M_0}{B_0} - 2))$	$c_1^{s_z}(k_z = 0) = 0$ $c_1^{s_z}(k_z = \pi) = 1$	SWI=1	FKM=1	(1 000001)
$-1 < \frac{M_0}{B_0} < 1$	$(\pi, 0, \pm \cos^{-1}(\frac{M_0}{B_0}))$ $(0, \pi, \pm \cos^{-1}(\frac{M_0}{B_0}))$	$c_1^{s_z}(k_z = 0) = -1$ $c_1^{s_z}(k_z = \pi) = 1$	SWI=2	FKM=0	(2 0000-11)
$1 < \frac{M_0}{B_0} < 3$	$(0, 0, \pm \cos^{-1}(\frac{M_0}{B_0} - 2))$	$c_1^{s_z}(k_z = 1) = 0$ $c_1^{s_z}(k_z = \pi) = 0$	SWI=1	FKM=1	(1 000010)

TABLE I. Topologically non-trivial phases of the 3D BHZ Hamiltonian. The SW points appear on the four  $k_z$  axis, and due to TRS, in pairs of opposite chirality. The first and the third phase have non-trivial FKM invariant and SWI of 1, while the middle phase has trivial FKM invariant with a SWI of 2. The vector of spin invariants appears in the last column.

where  $\sigma_x$  is the Pauli matrix. Deriving with respect to  $k_z$  and replacing  $k_z = \cos^{-1}(\frac{M_0}{B_0})$  we obtain the  $k_z$ -linear term of the SV matrix:

$$M_{s_z} \sim \frac{B_0}{D_0} (k_z - \cos^{-1}(\frac{M_0}{B_0})) \sigma_x. \quad (35)$$

Note that when  $D_0$  goes to zero, the slope of the SV spectrum goes to infinity, and the anticommutator of the spin and the Hamiltonian goes to zero. This fact is further explored in Fig. 3.

Similar calculations can be performed for the  $k_x$  and  $k_y$  linear expansions, thus showing that the SV eigenvalues are linear on  $\mathbf{k}$  around the SW points

When the structural constants are  $M_0 = 0, B_0 = A_0 = D_0 = 1$ , one can show that

$$M_{s_z} \sim k_x \sigma_z + k_y \sigma_y + (k_z - \cos^{-1}(\frac{M_0}{B_0})) \sigma_x, \quad (36)$$

thus implying that the SW points have chirality  $\pm 1$  and that the SV operator behaves like a  $\mathbf{k} \cdot \mathbf{p}$  Hamiltonian.

### B. Zeeman effect

Consider the BHZ Hamiltonian subject to an external magnetic field in the spin direction

$$H(\mathbf{k}) = H_{\text{BHZ}}(\mathbf{k}) + \mathbf{B}\hat{S}_z. \quad (37)$$

The energy eigenvalues of the two valence states become

$$\lambda = -\sqrt{\pm 2\sqrt{\mathbf{B}^2(M^2 + |A|^2) + M^2 + |A|^2 + D^2 + \mathbf{B}^2}}, \quad (38)$$

and one can see that there are Weyl type degenerate eigenstates whenever  $|A| = 0 = M$ . The same relations were found while solving equations (27–30) for the position of the SW points in the BHZ Hamiltonian. Therefore the SW points in the BHZ Hamiltonian, in the presence of a strong magnetic field aligned with the spin direction, evolve into energy Weyl points.

### C. Spin Weyl indicator

The three nontrivial topological phases of the 3D BHZ Hamiltonian could be read from the amount of SW points present in the system. The first and third phases provide examples of TIs with non-trivial FKM invariants, thus making them strong TIs, while the second one has trivial FKM invariant but its SW indicator is equal to 2.

The FKM invariant can be read from the eigenvalues of the Inversion operator on the 8 TRIMs. The Inversion operator acts via the diagonal matrix  $\text{diag}(1, -1, 1, -1)$  and the eigenvalues can be seen in Fig. 2. The parity of the number of pairs of negative eigenvalues on the 8 TRIMs is the FKM invariant, and one can see in Fig. 2 that the second phase has trivial FKM invariant. Calculating the first Chern class of the negative SV eigenstates across the planes  $k_z = 0$  and  $k_z = \pi$  we see that the absolute value of the difference of these Chern numbers is precisely the SWI. The information has been summarized in Table I.

### D. Spin Hall effect

It is known that the spin Hall conductivity (SHC) within the energy band gap is a way to classify the charge-spin transport response in topological insulator materials. For 2D TI, the SHC takes a constant value within the band gap, and in ideal cases like the Kane-Mele model, it becomes quantized (QSHE).<sup>33</sup> In real materials, the inclusion of SOC induces spin mixing, breaking the commutativity between the spin and Hamiltonian operators, thereby resulting in a non-quantized value for the SHC within the energy gap.<sup>34,35</sup> Despite this fact, the spin Chern numbers,<sup>12</sup> and therefore the SWI included in the last section, are well-defined quantities even in the

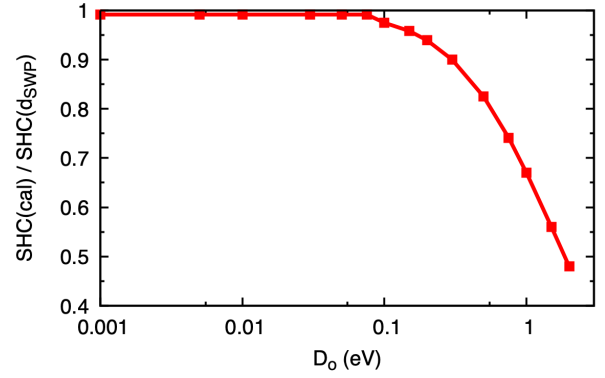


FIG. 3. Spin Hall conductivity calculated with the Kubo formula (41) divided by the spin Hall conductivity calculated from the distance of the SW points in the reciprocal space (39) as a function of the SOC strength  $D_0$  of the 3D BHZ model (16). It is noted that the SHE inside the bang gap is proportional to the SW point distance in the negligible SOC limit.

presence of SOC. Therefore, the SWI is a quantity that permits to enhance the characterization of the underlying properties of the system.

In 3D TIs, the characterization of non-trivial SHC within the band gap by topological invariants is still an active area of research. The 3D BHZ Hamiltonian presented above offers a promising model to understand this relation. By performing SHC calculations for the 3D BHZ model (see Fig. 3), we have found that in the limit of minimal spin mixing (corresponding to a small  $D_0$  term in the Hamiltonian (16)), the SHC becomes directly proportional to the proportion of  $k$ -layers in the reciprocal space with spin Chern numbers equal to 1. This also permits to detect a relationship between the SHC and the distance between SW points, generalizing the well established relation between the AHC and the distance between energy Weyl points.<sup>36</sup> In the case of the two SW points in the third non-trivial phase of the 3D BHZ model, the SHC inside the band gap can be calculated as:<sup>37</sup>

$$\sigma_{ij}^z = -\frac{\hbar}{2e} \frac{e^2 b_z}{2\pi^2 \hbar} \quad (39)$$

where  $2b_z = 2\cos^{-1}(\frac{M_0}{B_0} - 2)$  is the distance between the SW points in the reciprocal space. When considering the a finite spin mixing term in real materials, it becomes evident that the SHC presents a constant and non-quantized value within the energy gap, influenced by the strength of the SOC. This observation is depicted in Fig. 3.

### V. TIGHT BINDING MODEL

The spin Weyl indicator can also be incorporated in tight-binding (TB) models for 3D TIs. We have carried



out an extensive calculation on the TB model of the pristine pyrochlore model as was introduced by Varnava and Vanderbilt.<sup>17</sup> In this particular case it is well known that the TB model defines a 3D TI and its Hamiltonian has the following form:

$$H = -t \sum_{\langle i,j \rangle, \sigma} \hat{c}_{i\sigma}^\dagger \hat{c}_{j\sigma} + i\lambda \sum_{\langle\langle i,j \rangle\rangle, \alpha\beta} \nu_{ij} \hat{c}_{i\alpha}^\dagger \sigma_{\alpha\beta} \hat{c}_{j\beta} \quad (40)$$

where the first term represents the nearest-neighbor hopping interaction, while the second term represents the intrinsic SOC interaction (characterized by the coupling strength  $\lambda$ ). In this context,  $\sigma_i$  represents the Pauli matrices, while  $\nu_{ij}$  is determined by the cross product of  $\mathbf{b}_{ij} \times \mathbf{d}_{ij}$  with  $\mathbf{d}_{ij}$ . Here  $\mathbf{d}_{ij}$  is the unit vector connecting site  $i$  with site  $j$ , and  $\mathbf{b}_{ij}$  is the unit vector from the center of a tetrahedron to the midpoint of the bond  $\langle ij \rangle$ . This model is exactly the one that appears in the reference.<sup>17</sup> (§3).

This model exhibits a 3D TI that maintains time-reversal and inversion symmetry. By setting the parameter  $\lambda=0.3t$ , we computed the band structure at half-filling, revealing a bandgap of approximately 1.0 eV, as depicted in Fig. 4. We observed the emergence of two SW points along the  $-\Gamma$ - $\Gamma$ - $\Gamma$  path in the BZ, indicating the presence of these novel spin topological indicators. TB calculations along different  $k$ -paths revealed that the energy and SV spectrum are gapped in other regions of the BZ.

This system exhibits a spin Chern number transition along planes perpendicular to both the  $k_x$  and the  $k_y$  axis. The presence of SW points in the bulk is inferred from the SCN signal along the  $k_x$  and  $k_y$  axis as shown in Fig. 4 c). Fig. 4 f) depicts the position of the SW points with opposite chirality that produces the SCN signal in the system. This system models a SWTI with  $\text{SWI}=1$ , confirming the Strong Topological Insulating property of the pyrochlore lattice shown in.<sup>38,39</sup> The spin Invariants vector for the TB model is  $(1|10-1000)$ .

## VI. MATERIALS REALIZATION

We have calculated the spin invariants presented above in real materials, and we have focused our attention to  $\text{Bi}_2\text{Te}_3$  which is a 3D STI, and  $\text{SnTe}$ , which exhibits a distinct spin Weyl topological insulating property. The first material is modeled in a rhombohedral unit cell and consist of two layers of Bi atoms and three layers of Te/Se atoms, arranged in a quintuple layer structure. The coupling between atomic layers within one quintuple layer is strong, but much weaker between two quintuple layers.<sup>40</sup> The electronic band structure of  $\text{Bi}_2\text{Te}_3$  in the rhombohedral crystal structure is shown in Fig. 5a). The material exhibits an indirect band gap energy of approximately 0.2 eV.

In the SV spectrum shown in Fig. 5b) we observe the presence of two SW points along the  $\Gamma$ - $\Gamma$ - $\Gamma$   $k$ -path, cor-

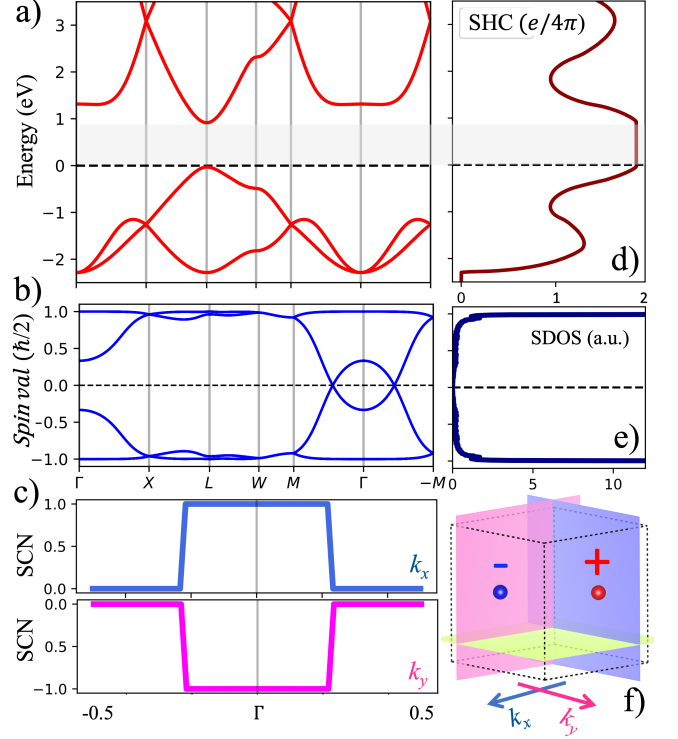


FIG. 4. Tight-binding model introduced in<sup>17</sup> with the Hamiltonian of Eqn. (40) and  $\lambda=0.3t$ . (a) Bulk band structure and (b) spin valence spectrum along high symmetry lines in the BZ. (c) spin Chern number (SCN) calculated for perpendicular planes along the  $k_x$  and  $k_y$  reciprocal axis, (d) spin Hall conductivity and (e) spin density of states as a function of the Fermi energy of the tight-binding model. f) Position of the spin Weyl points in the reciprocal space with the  $k$ -planes used for the SCN calculation.

responding to the main diagonal of the BZ. As depicted in Fig. 5e), the spin density of states reveals that the eigenvalues of the spin valence operator are concentrated around  $\pm 1$  values, except at the SW points. These SW points exhibit opposite chirality and give rise to a transition of the SCN when scanned across perpendicular  $k$ -planes in the reciprocal lattice. From Fig. 5c) it is noted that the SCN changes precisely at the positions of the SW points, signifying a topological transition between distinct planes of reciprocal space.

The topological nature of  $\text{Bi}_2\text{Te}_3$  is evident in our SHC calculation, where a non-zero signal in Fig. 5d) is observed within the band gap. This material can be classified by a  $\text{SWI}=1$ , in agreement with the Fu-Kane-Mele invariant of 1. This indicator is obtained from the calculation of Wilson loops on the  $k_l=0, \pi$  planes, corresponding to 0 and 1 respectively. The position and chirality of the SW points can be inferred from the change of the topological index of 0 at  $k_l=0$  to 1 at  $k_l=\pi$  along each  $k_l$  direction (See Fig. 5c), and its spin invariant vector becomes  $(1|101010)$ .

On the other hand, the  $\text{SnTe}$  exhibits a rocksalt crystal



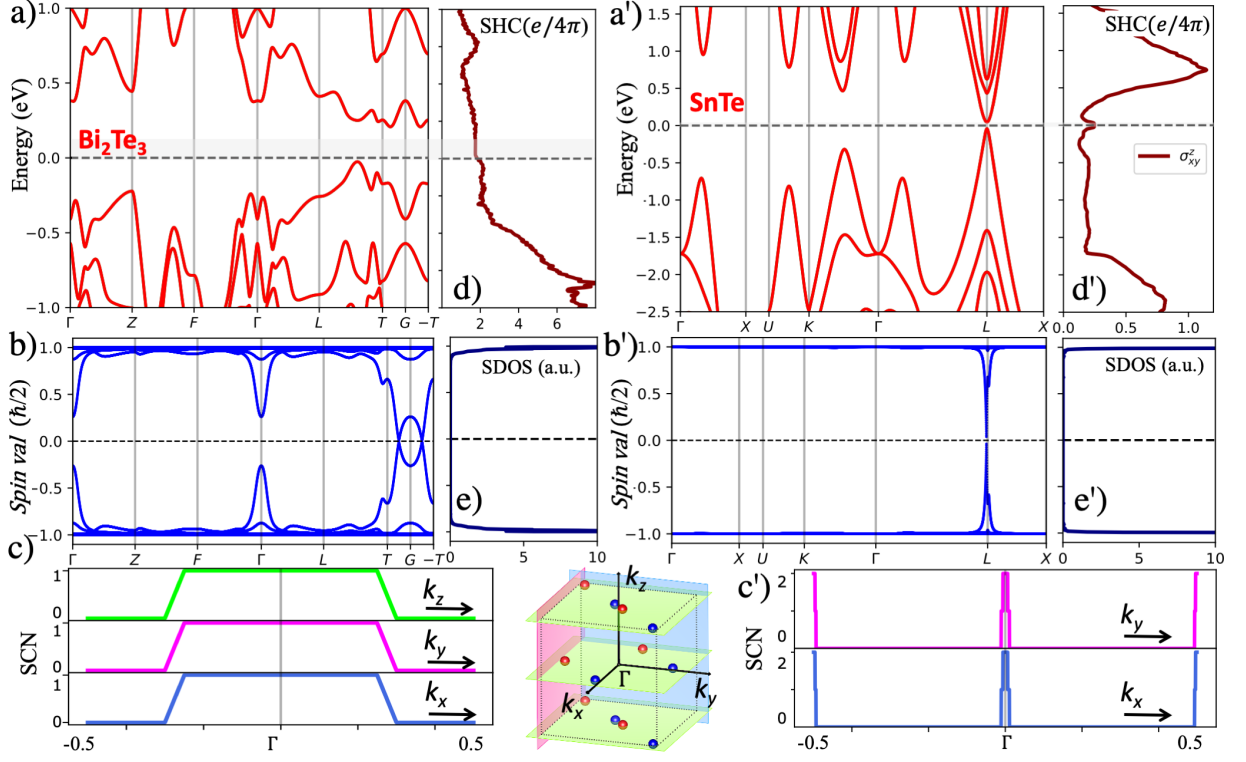


FIG. 5. (a) and (a') Bulk band structure, (b) and (b') spin valence spectrum along high symmetry lines in the BZ, (c) and (c') spin Chern number -SCN- calculated for perpendicular planes along the  $k_x$ ,  $k_y$  and  $k_z$  reciprocal axis, (d) and (d') spin Hall conductivity, (e) and (e') spin density of states as a function of the Fermi energy of the 3D topological materials  $\text{Bi}_2\text{Te}_3$  and  $\text{SnTe}$ . The central panel at the bottom presents the position of the eight SW points of  $\text{SnTe}$  with their chiralities.

structure with two atoms by unit-cell,<sup>41</sup> and its band gap of around 0.1 eV is located at four equivalent L points within the face-centered-cubic BZ as can be seen in Fig. 5a'). Despite the trivial FKM invariant calculation predicting a trivial character for  $\text{SnTe}$ , this material was previously classified as a crystalline topological insulator based on the presence of a non-trivial mirror Chern number.<sup>41</sup> Our findings have been corroborated by the observation of a non-zero SHC within the band gap, as shown in Fig. 5d').

From the SV spectrum presented in Fig. 5b'), eight SW points are detected close to the L and T points inducing a change of SCN as presented in Fig. 5c'). Accordingly, this material is classified by a SWI=4. The existence of these SW points serves as an indication of the transition in the internal topological phase along the  $k_x$ ,  $k_y$  and  $k_z$  directions. This transition involves a shift from a spin Chern number of 2 at the planes  $k_x = 0$  and  $k_y = 0$  to 0 in the interior of the interval  $(0, \pi)$ , to again a shift back to 2 across the planes  $k_x = \pi$  and  $k_y = \pi$ . This feature confirms the SWTI nature of  $\text{SnTe}$ , but more importantly, it highlights a significant difference from the conventional classification of  $\text{SnTe}$  using the Fu-Kane-Mele invariant. Here is worth mentioning that knowing the spin Chern number of the system along the planes  $k_l=0, \pi$  is not enough to distinguish its topological nature. In the particular case of  $\text{SnTe}$ , the spin

Chern numbers along the planes  $k_l=0, \pi$  for  $l = x, y$  is 2, while along the planes  $k_z=0, \pi$  is 0. One could mistake this material as a SCI, since the spin Chern numbers are equal along parallel planes  $k_l=0, \pi$ . Nevertheless, its correct classification is being an SWTI with spin invariants vector equal to  $(4|22200)$ .

Finally, Table II presents a summary of the 3D trivial and topological insulator materials studied in this work. The table includes the number of spin Weyl points, the spin Weyl indicator, the Fu-Kane-Mele invariant, the spin invariants vector, and the respective (time-reversal and inversion) symmetries associated with each material. We have considered representative examples from different 3D insulator materials to highlight the classification presented in Fig. 1.  $\text{Te}$ ,  $\text{GaAs}$ ,  $\text{AuF}_3$ , and  $\text{CaMnO}_3$  display trivial insulator behavior with energy and spin gaps. In contrast, Bismuth ( $\text{Bi}$ ) exhibits a constant spin Chern number of 2 along three directions in the BZ, indicating its classification as a spin Chern insulator. This is consistent with previous theoretical investigations that have demonstrated the presence of a 3D topological band structure in  $\text{Bi}$ .<sup>42</sup>

The spin Weyl indicator confirms that the material  $\text{Bi}_2\text{Se}_3$  exhibits a strong topological character similar to  $\text{Bi}_2\text{Te}_3$ , consistent with previous theoretical and experimental studies.<sup>40,43</sup> Finally, material  $\text{SnTe}$  exhibits a spin Weyl topological insulator property having eight SW

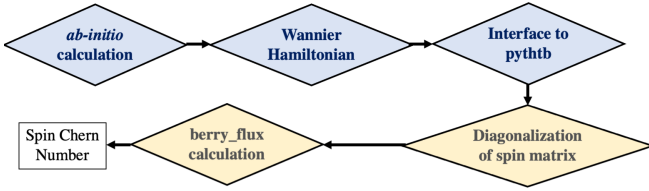


FIG. 6. Workflow showing the computational method. Ab-initio calculations (VASP code) are used to find the electronic structure of the material. Subsequently, the `wannier90` code is utilized to construct the wannier Hamiltonian, which serves as a basis for the generation of the tight-binding model using the `pythtb-wannier90` interface. The next step involves the generation of the spin matrix operator for valence states, followed by its diagonalization to obtain the spin valence spectrum. Finally, the Berry curvature is integrated over 2D  $k$ -planes to determine the spin Chern number.

points in the bulk; and whose distribution can be seen in the central-bottom panel of Fig. 5. This material has a trivial FKM invariant but Fig. 5d') shows that it exhibits a non-zero SHC inside the band gap. Therefore we claim that the SWI is more suited to detect SHC signals in 3D topological insulator materials.

Here it is worth mentioning that the properties of the spin Chern number and spin Weyl points in topological insulators remain valid when TRS invariance is broken. This is shown in the case of  $\text{CaMnO}_3$  and  $\text{MnBi}_2\text{Te}_4$ , where the collinear antiferromagnetic phase with Neel vector along the  $z$ -axis was considered (see Table 1). The topological invariant vector confirms the predicted topological response in  $\text{MnBi}_2\text{Te}_4$ , as reported in previous works.<sup>44,45</sup>

## VII. COMPUTATIONAL DETAILS

We used density-functional theory (DFT) calculations to investigate the spin topology of magnetic and nonmagnetic materials. The generalized gradient approximation (GGA),<sup>46</sup> as implemented in the Vienna *ab-initio* simulation package (VASP),<sup>47</sup> was used to account for exchange and correlation effects. In the electronic structure calculations, we expanded the electron wave function in plane waves with a cutoff energy of 520 eV. The Brillouin zone was sampled using a  $k$ -mesh of 0.03 ( $2\pi/\text{\AA}$ )  $k$ -space resolution. The lattice constants for the studied materials were obtained from the Materials Project database.<sup>48</sup>

We employed the `wannier90` code to build the maximally localized Wannier basis<sup>49</sup> as a post-processing approach following the DFT calculations. The `pythtb-wannier90` interface of the `pythtb` code<sup>50</sup> was utilized to generate tight-binding Hamiltonians for the TB model and for each material. Next, we used the electron wave functions of the valence states to generate the spin valence matrix operator and performed its diagonalization to obtain the spin valence spectrum. To study the spin topological properties, we used the

spin valence eigenvectors to integrate the Berry curvature (`berry-flux` utility in `pythtb`)<sup>50</sup> over 2D  $k$ -planes, thereby extracting spin Chern numbers across the Brillouin Zone. The workflow of this method is shown in Fig. 6.

The intrinsic spin Hall conductivity was calculated using the `WannierBerri` code<sup>51</sup> by integrating the spin Berry curvature over the first Brillouin zone. For the case of SHC ( $\sigma_{xy}^z$ ) we set:

$$\sigma_{xy}^z = -\frac{e^2}{\hbar} \sum_n \int_{BZ} \frac{dk^3}{(2\pi)^3} f_n(k) \Omega_{xy}^z(k) \quad (41)$$

where  $f_n(k)$  is the Fermi-Dirac distribution and the Berry curvature  $\Omega_n^z(k)$  for the  $n$ th band is:

$$\Omega_{xy}^z(k) = -2\hbar^2 \text{Im} \sum_{m \neq n} \frac{\langle \psi_n | \hat{j}_x^z | \psi_m \rangle \langle \psi_m | \hat{v}_y | \psi_n \rangle}{(\epsilon_{n,k} - \epsilon_{m,k})^2} \quad (42)$$

where  $|\psi_n(k)\rangle$  are the Bloch functions of a single band  $n$ ,  $k$  is the Bloch wave vector,  $\epsilon_{n,k}$  is the band energy,  $\hat{v}_i$  is the velocity operator in the  $i$  direction and  $\hat{j}_x^z = \frac{1}{2}\{\hat{v}_x, \hat{s}_z\}$  is the spin current operator. It is important to note that the  $\hat{j}_x^z$  definition does not incorporate the spin torque contributions, which is taken into account when the universal spin current operator is used.<sup>52</sup> Finally, the FKM index was computed using the `WannierTools` code.<sup>53</sup>

## VIII. CONCLUSIONS

We have found that 3D topological insulators (TI) can be identified by the presence of spin Weyl points in their spin valence spectrum or by the non-triviality of the spin Chern numbers. Both indicators serve as novel predictors of topological insulating phases. It is important to note that these phenomena cannot be regarded simply as a stack of two-dimensional states, thus making these indicators truly 3-dimensional. In addition, we have found a correlation between the presence of spin Weyl points in 3D TIs and the topological signal of the spin Hall effect (SHE) for the 3D BHZ model.

We propose the use of the spin invariants vector to enhance the topological classification of 3D materials. This vector contains the information regarding the spin Weyl indicator, and the values of the spin Chern numbers of the negative spin valence eigenvectors across the planes  $k_l=0,\pi$  for  $l=x,y,z$ . This vector contains the necessary information to distinguish the material as a spin insulator, a spin Chern insulator or a spin Weyl topological insulator. We have provided an array of materials which exhibit interesting spin topology phases and whose spin invariants vector predicts its topological nature.

The novelty of the spin invariants vector is shown when applied to Bismuth and  $\text{SnTe}$ . In the former case the material exhibits a spin Chern insulating property, while the

Material	SW points	SWI	FKM Inv.	Spin inv. vec.	TRS	Inversion symm.	Spin top. class.
Te	0	0	0	(0 000000)	✓	$X$	SI
GaAs	0	0	0	(0 000000)	✓	$X$	SI
AuF <sub>3</sub>	0	0	0	(0 000000)	✓	$X$	SI
Bi <sup>42</sup>	0	0	0	(0 222222)	✓	✓	SCI
Bi <sub>2</sub> Te <sub>3</sub> <sup>40</sup>	2	1	1	(1 101010)	✓	✓	STI
Bi <sub>2</sub> Se <sub>3</sub> <sup>43</sup>	2	1	1	(1 101010)	✓	✓	STI
SnTe <sup>41</sup>	8	4	0	(4 222200)	✓	✓	SWTI
CaMnO <sub>3</sub>	0	0	0	(0 000000)	$X$	✓	SI
MnBi <sub>2</sub> Te <sub>4</sub> <sup>44,45</sup>	2	1	1	(1 -1010-10)	$X$	✓	STI

TABLE II. spin topology calculated for 3D materials. spin Weyl points, spin Weyl indicator, Fu-Kane-Mele index, spin invariants vector, time-reversal and inversion symmetry, and spin topology classification according to Fig. 1. Bismuth (Bi) has a constant spin number of 2 along three directions of the BZ. MnBi<sub>2</sub>Te<sub>4</sub> and CaMnO<sub>3</sub> were calculated in the collinear antiferromagnetic phase with Neel vector along the  $z$ -axis.

former shows a spin Weyl topological insulating property. In both cases, the new invariant permits to carry out a precise classification of these with regards to their spin properties.

We believe that the spin invariants vector adds information to the characterization of the topological classification of materials, enhancing the known invariants and detecting new spin topological phases. Nevertheless, the relation of the spin invariants vector with the whole package of electromagnetic properties stills needs to be investigated.

## ACKNOWLEDGMENTS

The first author gratefully acknowledges the computing time granted on the supercomputer Mogon at Johannes Gutenberg University Mainz (hpc.uni-mainz.de). The second author acknowledges the support of CONACYT through project CB-2017-2018-A1-S-30345-F-3125 and of the Max Planck Institute for Mathematics in Bonn, Germany. Both authors thank the continuous support of the Alexander Von Humboldt Foundation, Germany.

- 
- [1] M. Z. Hasan and C. L. Kane. Colloquium: Topological insulators. *Rev. Mod. Phys.*, 82:3045–3067, Nov 2010.
  - [2] Xiao-Liang Qi and Shou-Cheng Zhang. Topological insulators and superconductors. *Rev. Mod. Phys.*, 83:1057–1110, Oct 2011.
  - [3] D. J. Thouless, M. Kohmoto, M. P. Nightingale, and M. den Nijs. Quantized hall conductance in a two-dimensional periodic potential. *Phys. Rev. Lett.*, 49:405–408, Aug 1982.
  - [4] Xiao-Liang Qi, Taylor L. Hughes, and Shou-Cheng Zhang. Topological field theory of time-reversal invariant insulators. *Phys. Rev. B*, 78:195424, Nov 2008.
  - [5] Andrew M. Essin, Joel E. Moore, and David Vanderbilt. Magnetoelectric polarizability and axion electrodynamics in crystalline insulators. *Phys. Rev. Lett.*, 102:146805, Apr 2009.
  - [6] A. Alexandradinata, Xi Dai, and B. Andrei Bernevig. Wilson-loop characterization of inversion-symmetric topological insulators. *Phys. Rev. B*, 89:155114, Apr 2014.
  - [7] Adrien Bouhon, Annica M. Black-Schaffer, and Robert-Jan Slager. Wilson loop approach to fragile topology of split elementary band representations and topological crystalline insulators with time-reversal symmetry. *Phys. Rev. B*, 100:195135, Nov 2019.
  - [8] Mikel Iraola, Juan L. Mañes, Barry Bradlyn, Matthew K. Horton, Titus Neupert, Maia G. Vergniory, and Stepan S. Tsirkin. Irrep: Symmetry eigenvalues and irreducible representations of ab initio band structures. *Computer Physics Communications*, 272:108226, 2022.
  - [9] Feng Tang, Hoi Chun Po, Ashvin Vishwanath, and Xiang-gang Wan. Comprehensive search for topological materials using symmetry indicators. *Nature*, 566(7745):486–489, Feb 2019.
  - [10] Barry Bradlyn, L. Elcoro, Jennifer Cano, M. G. Vergniory, Zhijun Wang, C. Felser, M. I. Aroyo, and B. Andrei Bernevig. Topological quantum chemistry. *Nature*, 547(7663):298–305, Jul 2017.
  - [11] Luis Elcoro, Benjamin J. Wieder, Zhida Song, Yuanfeng Xu, Barry Bradlyn, and B. Andrei Bernevig. Magnetic topological quantum chemistry. *Nature Communications*, 12(1):5965, Oct 2021.
  - [12] Emil Prodan. Robustness of the spin-chern number. *Phys. Rev. B*, 80:125327, Sep 2009.
  - [13] Xiangang Wan, Ari M. Turner, Ashvin Vishwanath, and Sergey Y. Savrasov. Topological semimetal and fermi-arc surface states in the electronic structure of pyrochlore iridates. *Phys. Rev. B*, 83:205101, May 2011.
  - [14] Hassan Shapourian and Taylor L. Hughes. Phase diagrams of disordered weyl semimetals. *Phys. Rev. B*, 93:075108, Feb 2016.
  - [15] Hoi Chun Po, Haruki Watanabe, and Ashvin Vishwanath. Fragile topology and wannier obstructions. *Phys. Rev. Lett.*, 121:126402, Sep 2018.
  - [16] B. Andrei Bernevig, Taylor L. Hughes, and Shou-Cheng Zhang. Quantum spin hall effect and topolog-

- ical phase transition in hgte quantum wells. *Science*, 314(5806):1757–1761, 2006.
- [17] Nicodemos Varnava and David Vanderbilt. Surfaces of axion insulators. *Phys. Rev. B*, 98:245117, Dec 2018.
- [18] Gunnar F. Lange, Adrien Bouhon, and Robert-Jan Slager. Spin texture as a bulk indicator of fragile topology. *Phys. Rev. Res.*, 5:033013, Jul 2023.
- [19] Hiromu Araki, Takahiro Fukui, and Yasuhiro Hatsugai. Entanglement chern number for three-dimensional topological insulators: Characterization by weyl points of entanglement hamiltonians. *Phys. Rev. B*, 96:165139, Oct 2017.
- [20] Lin Kuan-Sen, Palumbo Giandomenic, Guo Zhaopeng, Hwang Yoonseok, Blackburn Jeremy, Shoemaker Daniel P., Mahmood Fahad, Wang Zhijun, Fiete Gregory A., Wieder Benjamin J., and Bradlyn Barry. Spin-resolved topology and partial axion angles in three-dimensional insulators. *arXiv preprint*, page 2207.10099, 2023.
- [21] David Vanderbilt. *Berry Phases in Electronic Structure Theory: Electric Polarization, Orbital Magnetization and Topological Insulators*. Cambridge University Press, 2018.
- [22] Roderich Moessner and Joel E. Moore. *Topological Phases of Matter*. Cambridge University Press, 2021.
- [23] Tiantian Zhang, Yi Jiang, Zhida Song, He Huang, Yuqing He, Zhong Fang, Hongming Weng, and Chen Fang. Catalogue of topological electronic materials. *Nature*, 566(7745):475–479, Feb 2019.
- [24] M. G. Vergniory, L. Elcoro, Claudia Felser, Nicolas Regnault, B. Andrei Bernevig, and Zhijun Wang. A complete catalogue of high-quality topological materials. *Nature*, 566(7745):480–485, Feb 2019.
- [25] Qian Niu, D. J. Thouless, and Yong-Shi Wu. Quantized hall conductance as a topological invariant. *Phys. Rev. B*, 31:3372–3377, Mar 1985.
- [26] Liang Fu, C. L. Kane, and E. J. Mele. Topological insulators in three dimensions. *Phys. Rev. Lett.*, 98:106803, Mar 2007.
- [27] Ke He, Yayu Wang, and Qi-Kun Xue. Topological materials: Quantum anomalous hall system. *Annual Review of Condensed Matter Physics*, 9(1):329–344, 2018.
- [28] Liang Fu and C. L. Kane. Time reversal polarization and a  $Z_2$  adiabatic spin pump. *Phys. Rev. B*, 74:195312, Nov 2006.
- [29] Rafael González-Hernández, Carlos Pinilla, and Bernardo Uribe. Axion insulators protected by  $C_2T$  symmetry, their  $k$ -theory invariants, and material realizations. *Phys. Rev. B*, 106:195144, Nov 2022.
- [30] Yingxi Bai, Linke Cai, Ning Mao, Runhan Li, Ying Dai, Baibiao Huang, and Chengwang Niu. Doubled quantum spin hall effect with high-spin chern number in  $\alpha$ -antimonene and  $\alpha$ -bismuthene. *Phys. Rev. B*, 105:195142, May 2022.
- [31] Dongchao Wang, Li Chen, Changmin Shi, Xiaoli Wang, Guangliang Cui, Pinhua Zhang, and Yeqing Chen. Quantum spin hall insulator in halogenated arsenene films with sizable energy gaps. *Scientific Reports*, 6(1):28487, Jun 2016.
- [32] H.B. Nielsen and M. Ninomiya. Absence of neutrinos on a lattice: (i). proof by homotopy theory. *Nuclear Physics B*, 185(1):20 – 40, 1981.
- [33] Liang Fu, C. L. Kane, and E. J. Mele. Topological insulators in three dimensions. *Phys. Rev. Lett.*, 98:106803, Mar 2007.
- [34] Filipe Matusalem, Marcelo Marques, Lara K. Teles, Lars Matthes, Jürgen Furthmüller, and Friedhelm Bechstedt. Quantization of spin hall conductivity in two-dimensional topological insulators versus symmetry and spin-orbit interaction. *Phys. Rev. B*, 100:245430, Dec 2019.
- [35] S. M. Farzaneh and Shaloo Rakheja. Intrinsic spin hall effect in topological insulators: A first-principles study. *Phys. Rev. Mater.*, 4:114202, Nov 2020.
- [36] A. A. Burkov. Anomalous hall effect in weyl metals. *Phys. Rev. Lett.*, 113:187202, Oct 2014.
- [37] Yan Sun, Yang Zhang, Claudia Felser, and Binghai Yan. Strong intrinsic spin hall effect in the taas family of weyl semimetals. *Phys. Rev. Lett.*, 117:146403, Sep 2016.
- [38] H.-M. Guo and M. Franz. Three-dimensional topological insulators on the pyrochlore lattice. *Phys. Rev. Lett.*, 103:206805, Nov 2009.
- [39] Moyuru Kurita, Youhei Yamaji, and Masatoshi Imada. Topological insulators from spontaneous symmetry breaking induced by electron correlation on pyrochlore lattices. *Journal of the Physical Society of Japan*, 80(4):044708, 2011.
- [40] Y. L. Chen, J. G. Analytis, J.-H. Chu, Z. K. Liu, S.-K. Mo, X. L. Qi, H. J. Zhang, D. H. Lu, X. Dai, Z. Fang, S. C. Zhang, I. R. Fisher, Z. Hussain, and Z.-X. Shen. Experimental realization of a three-dimensional topological insulator,  $Bi_2Te_3$ . *Science*, 325(5937):178–181, 2009.
- [41] Timothy H. Hsieh, Hsin Lin, Junwei Liu, Wenhui Duan, Arun Bansil, and Liang Fu. Topological crystalline insulators in the snite material class. *Nature Communications*, 3(1):982, Jul 2012.
- [42] Frank Schindler, Zhijun Wang, Maia G. Vergniory, Ashley M. Cook, Anil Murani, Shamashis Sengupta, Alik Yu. Kasumov, Richard Deblock, Sangjun Jeon, Ilya Drozdov, Hélène Bouchiat, Sophie Guéron, Ali Yazdani, B. Andrei Bernevig, and Titus Neupert. Higher-order topology in bismuth. *Nature Physics*, 14(9):918–924, Sep 2018.
- [43] Haijun Zhang, Chao-Xing Liu, Xiao-Liang Qi, Xi Dai, Zhong Fang, and Shou-Cheng Zhang. Topological insulators in  $Bi_2Se_3$ ,  $Bi_2Te_3$  and  $Sb_2Te_3$  with a single dirac cone on the surface. *Nature Physics*, 5(6):438–442, Jun 2009.
- [44] Yujun Deng, Yijun Yu, Meng Zhu Shi, Zhongxun Guo, Zihan Xu, Jing Wang, Xian Hui Chen, and Yuanbo Zhang. Quantum anomalous hall effect in intrinsic magnetic topological insulator  $MnBi_2Te_4$ . *Science*, 367(6480):895–900, 2020.
- [45] Jiaheng Li, Yang Li, Shiqiao Du, Zun Wang, Bing-Lin Gu, Shou-Cheng Zhang, Ke He, Wenhui Duan, and Yong Xu. Intrinsic magnetic topological insulators in van der waals layered  $MnBi_2Te_4$ -family materials. *Science Advances*, 5(6):eaaw5685, 2019.
- [46] John P. Perdew, Kieron Burke, and Matthias Ernzerhof. Generalized gradient approximation made simple. *Phys. Rev. Lett.*, 77:3865–3868, Oct 1996.
- [47] G Kresse and J Furthmüller. Efficient iterative schemes for ab initio total-energy calculations using a plane-wave basis set. *Phys. Rev. B*, 54(16):11169–11186, oct 1996.
- [48] Anubhav Jain, Shyue Ping Ong, Geoffroy Hautier, Wei Chen, William Davidson Richards, Stephen Dacek, Shreyas Cholia, Dan Gunter, David Skinner, Gerbrand Ceder, and Kristin A. Persson. Commentary: The materials project: A materials genome approach to accelerating materials innovation. *APL Materials*, 1(1):011002, Mar 2007.

- 2013.
- [49] Arash A. Mostofi, Jonathan R. Yates, Giovanni Pizzi, Young-Su Lee, Ivo Souza, David Vanderbilt, and Nicola Marzari. An updated version of wannier90: A tool for obtaining maximally-localised wannier functions. *Computer Physics Communications*, 185(8):2309 – 2310, 2014.
  - [50] Python tight binding open-source package. <http://physics.rutgers.edu/pythtb>.
  - [51] Stepan S. Tsirkin. High performance wannier interpolation of berry curvature and related quantities with wannierberri code. *npj Computational Materials*, 7(1):33, Feb 2021.
  - [52] Junren Shi, Ping Zhang, Di Xiao, and Qian Niu. Proper definition of spin current in spin-orbit coupled systems. *Phys. Rev. Lett.*, 96:076604, Feb 2006.
  - [53] QuanSheng Wu, ShengNan Zhang, Hai-Feng Song, Matthias Troyer, and Alexey A. Soluyanov. Wannier-tools: An open-source software package for novel topological materials. *Computer Physics Communications*, 224:405 – 416, 2018.